The Astrophysical Journal, 616:1042–1057, 2004 December 1

A NEAR-INFRARED STUDY OF THE NGC 7538 STAR-FORMING REGION

D. K. Ojha,[1] M. Tamura, Y. Nakajima, and M. Fukagawa
National Astronomical Observatory of Japan, Mitaka, Tokyo 181-8588, Japan; ojha@tifr.res.in

K. Sugitani
Institute of Natural Sciences, Nagoya City University, Mizuho-ku, Nagoya 467-8501, Japan

C. Nagashima, T. Nagayama, T. Nagata, and S. Sato
Department of Astrophysics, Faculty of Sciences, Nagoya University, Chikusa, Nagoya 464-8602, Japan

S. Vig and S. K. Ghosh
Tata Institute of Fundamental Research, Homi Bhabha Road, Colaba, Mumbai 400 005, India

A. J. Pickles
Caltech Optical Observatories, California Institute of Technology, MS 105-24, Pasadena, CA 91125

M. Momose
Institute of Astrophysics and Planetary Sciences, Ibaraki University, Bunkyo 2-1-1, Mito, Ibaraki 310-8512, Japan

and

K. Ogura
Kokugakuin University, Higashi, Shibuya-ku, Tokyo 150-8440, Japan
Received 2004 April 16; accepted 2004 August 11

ABSTRACT

We present subarcsecond (FWHM $\sim 0\farcs7$), near-infrared (NIR) JHK_s-band images and a high-sensitivity radio continuum image at 1280 MHz, using SIRIUS on the University of Hawaii 88 inch (2.2 m) telescope and the Giant Metrewave Radio Telescope (GMRT). The NIR survey covers an area of $\sim$24 arcmin^2 with 10 σ limiting magnitudes of $\sim$19.5, 18.4, and 17.3 in the J, H, and K_s bands, respectively. Our NIR images are deeper than any JHK surveys to date for the larger area of the NGC 7538 star-forming region. We construct JHK color-color and $J - H/J$ and $H - K/K$ color-magnitude diagrams to identify young stellar objects (YSOs) and to estimate their masses. Based on these color-color and color-magnitude diagrams, we identified a rich population of YSOs (Class I and Class II) associated with the NGC 7538 region. A large number of red sources ($H - K > 2$) have also been detected around NGC 7538. We argue that these red stars are most probably pre–main-sequence stars with intrinsic color excesses. Most of the YSOs in NGC 7538 are arranged from the northwest toward the southeast regions, forming a sequence in age: a diffuse H II region (northwest and oldest, where most of the Class II and Class I sources are detected), a compact IR core (center), and regions with an extensive IR reflection nebula and a cluster of red young stars (southeast and south). We find that the slope of the K_s-band luminosity function of NGC 7538 is lower than the typical values reported for young embedded clusters, although equally low values have also been reported in the W3 Main star-forming region. From the slope of the K_s-band luminosity function and the analysis by Megeath and coworkers, we infer that the embedded stellar population is composed of YSOs with an age of $\sim$1 Myr. Based on the comparison of models of pre–main-sequence stars with the observed color-magnitude diagram, we find that the stellar population in NGC 7538 is primarily composed of low-mass pre–main-sequence stars similar to those observed in the W3 Main star-forming region. The radio continuum image from the GMRT observations at 1280 MHz shows an arc-shaped structure due to the interaction between the H II region and the adjacent molecular cloud. The ionization front at the interface between the H II region and the molecular cloud is clearly delineated by comparing the radio continuum, molecular line, and NIR images.

Subject headings: infrared: stars — ISM: clouds — ISM: individual (NGC 7538) — open clusters and associations: general — stars: formation — stars: pre–main-sequence

Online material: color figures

1. INTRODUCTION

The H II region NGC 7538, which is part of the Cas OB2 complex at a distance of 2.8 kpc (Blitz et al. 1982; Campbell & Thompson 1984), harbors massive stellar objects in various early stages of development (Campbell & Persson 1988 and references therein). The NGC 7538 star-forming region consists of an optically visible H II region and at least 11 high-luminosity infrared sources (NGC 7538 IRS 1–11), probably corresponding to young massive stars (Kameya et al. 1990). There are three major activity centers in NGC 7538; the northwest region contains IRS 4–8, the central region, IRS 1–3, and the southeast companion, IRS 9 (Werner et al. 1979). McCaughrean et al. (1991) discussed their near-infrared (NIR) images from a morphological perspective and suggested several different evolutionary stages in the NGC 7538 star-forming complex with considerable substructure. The central region

[1] On leave from the Tata Institute of Fundamental Research, Mumbai 400 005, India.

hosts a pair of ultracompact (UC) H II regions, NGC 7538A and NGC 7538B (Wood & Churchwell 1989). The far-infrared luminosity from IRS 1–3 in the central region is $2.5 \times 10^5\ L_\odot$ (Werner et al. 1979). The luminosity of IRS 9 is $4 \times 10^4\ L_\odot$. NGC 7538 IRS 1 is associated with a large variety of molecular maser species (Dickel et al. 1982; Kameya et al. 1990; Menten et al. 1986; Rots et al. 1981; Madden et al. 1986; Gaume et al. 1991). Very Large Array (VLA) radio observations were made by Rots et al. (1981) and Campbell (1984). Campbell (1984) presented strong evidence for the existence of a collimating disk around NGC 7538 IRS 1 and an associated outflow of ionized gas.

Momose et al. (2001) presented imaging polarimetry of the 850 μm dust continuum emission in the NGC 7538B region with the SCUBA Polarimeter on the James Clerk Maxwell Telescope (JCMT). They found two prominent cores associated with IRS 1 and IRS 11 in the surface brightness map of the continuum emission. The total cloud mass derived from the surface brightness map is $6.7 \times 10^3\ M_\odot$. The polarization map shows a striking difference between IRS 1 and IRS 11, suggesting that small-scale fluctuations of the magnetic field are more prominent in IRS 1. They interpreted this in terms of a difference in evolutionary stage of the cores. Inside IRS 1, which seems to be at a later evolutionary stage than IRS 11, substructures such as subclumps or a cluster of infrared sources have already formed. A 2 mm continuum mapping observation around NGC 7538 IRS 1–3 was made by Akabane et al. (2001) using the Nobeyama Bolometer Array (NOBA) mounted on the Nobeyama 45 m telescope. They derived a total cloud mass of about $6.9 \times 10^3\ M_\odot$, which is almost the same as that from Momose et al. (2001).

Bloomer et al. (1998) imaged the NGC 7538 IRS 1–3 region in various infrared wavelength bands. They studied in detail the infrared-bright knots due to very young O-type stars (IRS 1, 2, and 3) behind an extinction of at least $A_V = 16$ mag. They found a shell-like structure, which presumably corresponds to a shock caused by the high-velocity stellar wind from IRS 2 colliding with the surrounding molecular cloud. The K_s-bright source IRS 9 was discovered at the tip of the southeastern nebula and was identified as a protostellar object by Werner et al. (1979). There are powerful bipolar outflows from the three dominant IR sources in the region, IRS 1, IRS 9, and IRS 11 (Kameya et al. 1989; Davis et al. 1998), of which IRS 1 and IRS 11 are well-known OH maser sources. IRS 1 and IRS 9 are identified as the most likely powering sources of massive, bipolar CO outflows, based on the morphology and polarization of their associated NIR reflection nebulae (Tamura et al. 1991). Numerous H_2 features have been observed in the NGC 7538 region, in particular a collimated jet associated with the IRS 9 outflow, as well as possible bow shocks in both the IRS 1 and IRS 9 flows (Davis et al. 1998). These are closely associated with the bipolar CO outflows.

The high spatial resolution submillimeter maps show filamentary dust ridges extending from and connecting to the three major activity centers (IRS 1–3, IRS 11, and IRS 9) in the NGC 7538 star-forming cloud (Sandell & Sievers 2004). In addition to the three already known star formation centers, Sandell & Sievers (2004) find a fainter extended submillimeter source near IRS 4 inside the optical H II region. Sandell et al. (2003) reported the detection of a massive rotating disk around the high-mass Class 0 candidate NGC 7538S both in continuum and in molecular lines, about 80″ to the south of IRS 1. NGC 7538S is the strongest submillimeter continuum source in NGC 7538 (Sandell & Sievers 2004).

In this paper we present high-resolution *J*-, *H*-, and K_s-band observations over a large area ($\sim$24 arcmin^2) centered on IRS 1–3. To complement the NIR data and to understand the H II region more comprehensively, radio continuum observations were also obtained. As in our previous work on the W3 Main star-forming region (Ojha et al. 2004), our motivation is to look for new young stellar objects (YSOs) associated with the NGC 7538 region and to classify their evolutionary stages. From the slope of the K_s-band luminosity function (KLF), we discuss the age sequence and the mass spectrum of YSOs in the NGC 7538 region. In the case of W3 Main we found that the power-law slope of the KLF is lower than the typical values reported for embedded young clusters. Another motivation of this work is to compare the KLF slope of NGC 7538 with that of W3 Main to find any similarity or difference in the properties of the two high-mass star-forming regions and of the subregions within NGC 7538.

In § 2 we present the details of the observations and data reduction procedures. Section 3 contains the results and discussion on the mostly pointlike YSOs and describes the details of individual nebulosities and YSOs. We then summarize our conclusions in § 4.

2. OBSERVATIONS AND DATA REDUCTION

2.1. *NIR Observations*

The subarcsecond imaging observations of the NGC 7538 star-forming region in the NIR wavelengths *J* ($\lambda = 1.25$ μm), *H* ($\lambda = 1.63$ μm), and K_s ($\lambda = 2.14$ μm) were obtained on 2000 August 15 with the University of Hawaii 2.2 m telescope and SIRIUS (Simultaneous Three-Color Infrared Imager for Unbiased Surveys), equipped with three 1024×1024 HgCdTe arrays. The field of view (FOV) in each band is $\sim 4\farcm9 \times 4\farcm9$, with a pixel scale of 0.″28 at the f/10 Cassegrain focus. The HgCdTe arrays work linearly within 3% up to 15,000 ADU and saturate at $\sim$25,000 ADU (Nagayama et al. 2003). At $K_s = 12$ mag, the ADU counts are well below 15,000; thus, we consider the source magnitudes to be correct within 3%. Further details of the instrument are given in Nagashima et al. (1999) and Nagayama et al. (2003).

We obtained 27 dithered exposures of the target centered at $(\alpha, \delta) = (23^{\rm h}13^{\rm m}43\overset{\rm s}{.}95, +61^\circ28'44\farcs2)$ (J2000.0), each 20 s long, simultaneously for each band and nine dithered sky frames centered at $(\alpha, \delta) = (23^{\rm h}15^{\rm m}59\overset{\rm s}{.}60, +61^\circ28'44\farcs2)$ (J2000.0), which is $\sim$34′ east of the target position. The sky frame was also used as a reference field to assess the stellar populations within the NGC 7538 star-forming region (see § 3). Total on-target integration time in each of the bands was 9 minutes. All the observations were made under good photometric sky conditions. We found an rms magnitude fluctuation of less than 0.04 mag in the JHK_s bands during the NGC 7538 observations. The average seeing sizes (FWHM) in the *J*, *H*, and K_s bands were 0.″7, 0.″7, and 0.″6, respectively. The observations were made at air masses between 1.3 and 1.5. Dark frames and dome flats were obtained at the beginning and end of the observations. The photometric calibration was obtained by observing the standard star 9183 in the faint NIR standard star catalog of Persson et al. (1998) at air masses closest to the target observations. The *J*-, *H*-, and K_s-band images of the NGC 7538 star-forming region are shown in Figure 1.

Data reduction was done with the pipeline software based on NOAO's IRAF[2] package tasks. Dome flat-fielding and sky

[2] IRAF is distributed by the National Optical Astronomy Observatory, which is operated by the Association of Universities for Research in Astronomy, Inc., under contract to the National Science Foundation.

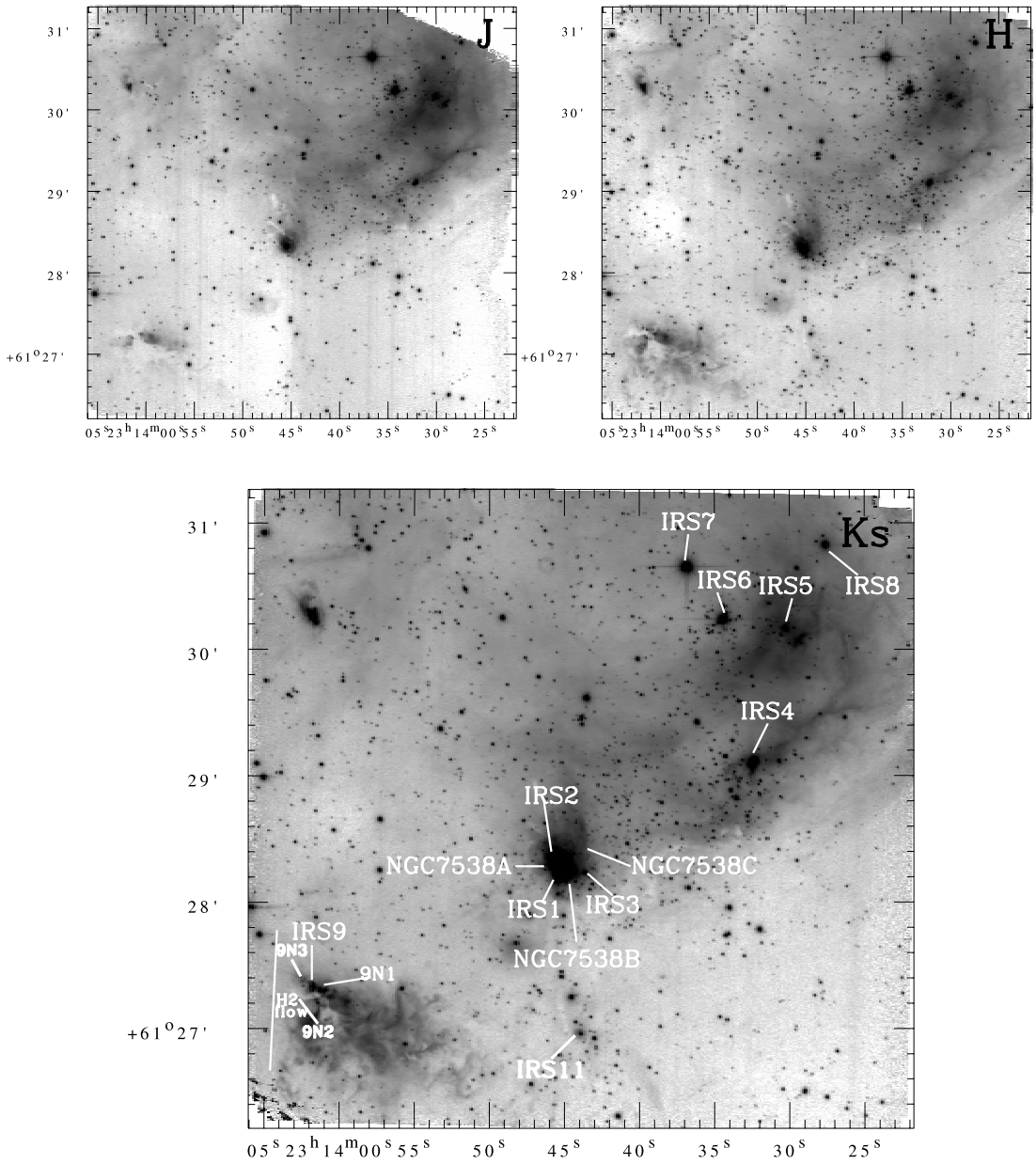

FIG. 1.—*J*-, *H*-, and K_s-band images of the NGC 7538 star-forming region displayed in a logarithmic intensity scale. The FOV is $\sim 4.'9 \times 4.'9$. The locations of the individual IR sources are marked in the K_s-band image. The direction of the NGC 7538 IRS 9 "H_2 flow" reported by Davis et al. (1998) is also indicated in the K_s-band image. North is up, and east is to the left. The abscissa and the ordinate are in the J2000.0 epoch.

subtraction with a median sky frame were applied. Identification and photometry of point sources were performed with the DAOFIND and DAOPHOT packages in IRAF, respectively. Because of source confusion and nebulosity within the NGC 7538 region, photometry was obtained using the point-spread function (PSF) algorithm ALLSTAR in the DAOPHOT package (Stetson 1987). For the JHK_s-band images the adopted fitting radii were 3 pixels ($\sim$1 FWHM of the PSF), and the PSF radius was 13 pixels. The local sky was evaluated in an annulus with an inner radius of 12 pixels and a width of 21 pixels. We used an aperture radius of 3 pixels ($\sim 0.''84$) with appropriate aperture corrections per band for the final photometry.

The resulting photometric data are in the SIRIUS system. For the purposes of plotting these data in color-color (CC) and color-magnitude (CM) diagrams, we have converted them into the California Institute of Technology (CIT) system using the color transformations between the SIRIUS and CIT systems (Nagashima et al. 2003),[3] which have been obtained by observing several of the red standard stars of Persson et al. (1998). Absolute position calibration was achieved using the coordinates of a number of stars from the Two Micron All Sky Survey (2MASS) catalog. The position accuracy is better than $\pm 0.''05$ rms in the NGC 7538 field.

The completeness limits of the images were evaluated by adding artificial stars of different magnitudes to the images and determining the fraction of these stars recovered in each magnitude bin. The recovery rate was greater than 90% for magnitudes brighter than 19, 18.5, and 17.5 in the *J*, *H*, and K_s bands, respectively. The observations are complete (100%) to the level of 17, 16, and 15 mag in the *J*, *H*, and K_s bands,

[3] Also available at http://www.z.phys.nagoya-u.ac.jp/~sirius/about/color_e.html.

respectively. The limiting magnitudes (at 10 σ) are estimated to be $\sim$19.5, 18.4, and 17.3 at the J, H, and K_s bands, respectively. We found that within the 10 σ detection limit, the accuracy on magnitudes of $\sim$98% of the stars in our sample is better than 0.2 mag. The sources are saturated at $K_s < 12$.

We estimated the errors in photometry due to source confusion and nebulosity through artificial star experiments. The difference between the magnitudes of the added and recovered stars should reflect the effect of confusion with other stars and the background nebulosity. We find that for $J = 19.5$, $H = 18.4$, and $K_s = 17.3$ stars (at our 10 σ magnitude detection limit), the rms error of the difference is 0.17, 0.15, and 0.14 mag, respectively. The rms error of the difference is 0.14, 0.15, and 0.15 mag, respectively, for $J = 19$, $H = 18.5$, and $K_s = 17.5$ stars (corresponding to the 90% completeness level). The error increases rapidly with increasing magnitude.

2.2. *GMRT Radio Continuum Observations*

The ionized gas within and around the H II region associated with the NGC 7538 star-forming region has been mapped at low and high angular resolutions using the Giant Metrewave Radio Telescope (GMRT) array in India. The radio continuum observations centered at $(\alpha, \delta) = (23^{\rm h}13^{\rm m}43^{\rm s}.95, +61^\circ28'44''.2)$ (J2000.0) were carried out at 1280 MHz on 2004 January 26. The source 3C 48 was used as the primary flux calibrator for the 1280 MHz observations, while the source 2355+498 was used as a secondary calibrator. The GMRT antennas and their configurations are discussed in detail by Swarup et al. (1991).

Data reduction was done in classic AIPS. Bad data (dead antennas, interference, spikes, etc.) were identified and flagged using UVFLG and TVFLG. Images of the field were formed by Fourier inversion and cleaning (IMAGR). The initial images were improved by self-calibration (CALIB) in both phase and amplitude.

Figure 2 shows the radio continuum image of the whole NGC 7538 region, generated from the GMRT interferometric observations at 1280 MHz. This image has a resolution of $22''.5 \times 12''.4$ and an rms of $\sim$4 mJy beam^{-1}. The total flux density is 13.1 Jy in the map. The inset in Figure 2 is a high-resolution GMRT map of the central radio peak. This image has a resolution of $6''.6 \times 4''.7$, an rms of $\sim$1.3 mJy beam^{-1}, and a total flux density of 978.7 mJy. The primary FOV at 1280 MHz is about $0^\circ.4$.

3. RESULTS AND DISCUSSION

3.1. *Prominent Infrared Nebulae*

A composite color image was constructed from the SIRIUS J-, H-, and K_s-band images (J represented in blue, H in green, and K_s in red) and is shown in Figure 3. The individual prominent IR sources are marked in the K_s-band image in Figure 1. The most prominent features are the diffuse purple-pink color to the northwest, the compact and bright orange color at the center, and the fluffy and dark orange color to the southeast. It is noteworthy that the scarce star field (*black*) extends to the southwest of the field, where the dense CO molecular cloud is located (see Fig. 4; Davis et al. 1998). We briefly describe the infrared appearance of the nebulae from a morphological perspective here, then discuss the pointlike sources in detail below.

The large diffuse emission extending to the northwest of IRS 1, 2, and 3 (see Fig. 3) is probably due to the combination of free-free and bound-free emission, corresponding to what is seen optically, and coincides well with the radio brightness from the GMRT observations at 1280 MHz shown in Figure 4. The extended filaments of H_2 line emission to the northwest of the IRS 1–3 cluster around the photodissociation regions at the interface between the H II and the molecular cloud are particularly striking (Fig. 5; Davis et al. 1998).

The bright and compact infrared nebula embedded with IRS 1, 2, and 3 at the center of Figure 3 (see also Fig. 12*a*) is coincident with the peak of the radio continuum, although the IRS sources remain unresolved with the GMRT. The radio peak in the center of the map in Figure 2 appears elongated northward by 60″. The high-resolution radio map (inset in Fig. 2) resolves this elongation into two lobes with a separation of 26″ in the north-south direction.

The fluffy nebula associated with IRS 9 is revealed $\sim$2′ southeast of IRS 1. A few red young stars are located at the easternmost tip of the nebula. The fluffy morphology, as well as the dark patches extending 70″ to the west, plausibly arises from reflection illuminated by these red sources (see Fig. 12*b*, § 3.8.2). The direction of the NGC 7538 IRS 9 "H_2 jet" reported by Davis et al. (1998) is indicated in Figure 5. Two small peculiar nebulosities are also revealed at the northeast corner in the composite image in Figure 3 and in the continuum-subtracted H_2 image in Figure 5. The enlarged view of this region is shown in Figure 12*d*.

The selected regions with individual IR sources and associated nebulosities are described in detail in § 3.8.

3.2. *Ionizing Sources of the* H II *Region*

In the diffuse H II region, there lie five radio peaks in Figure 4. Although three bright IRS sources lie therein, none of them coincide with any radio peaks. IRS 5, located close ($\sim$6″ northwest) to the brightest radio peak and assigned as an O9-type star in the $H - K$ versus K CM diagram (see Fig. 7; Moreno & Chavarria 1986), might be responsible for the nearby radio peak but is still insufficient to power the whole H II region. IRS 6, the brightest infrared source in the H II region, is located $\sim$27″ ($\sim$0.37 pc in projection) northeast of the brightest radio peak and is estimated to be an O6–O7 type from its color and IR luminosity (Wynn-Williams et al. 1974; Moreno & Chavarria 1986). IRS 7 has been identified as a K-type foreground star (Moreno & Chavarria 1986), and IRS 8 does not coincide with any optical or radio feature (Wynn-Williams et al. 1974). IRS 7 and IRS 8 are most probably not associated with the NGC 7538 nebula (Wynn-Williams et al. 1974; Zheng et al. 2001).

It is most plausible that IRS 6 is the main exciting source responsible for this H II region. However, the theoretical Strömgren radius of the H II region ionized by an O6-type star is roughly 15 times larger than the observed one (see Fig. 3). This means that the H II region is under expansion, and the central star (IRS 6) is at a very early stage of its evolution. However, the number of UV photons emitted by O stars dramatically changes with the spectral subclass. In addition, young O stars are often surrounded by some amount of dust, which attenuates the UV emission that ionizes the surrounding gas. As a result, the size of the Strömgren sphere is reduced compared to the ideal case. Therefore, the precise spectral type of the exciting star and information on the amount of surrounding dust are required for a quantitative discussion of the evolution of the NGC 7538 H II region.

In Figures 4 and 5, a cavity wall is apparent with a steep cliff of both CO and radio emission running from northwest to southeast (but with opposite gradients in the northeast/southwest direction) and a gradual decrease of the radio emission, as well as the Hα emission (see Moreno & Chavarria 1986), from southwest to northeast. At the cliff the H II region is plausibly

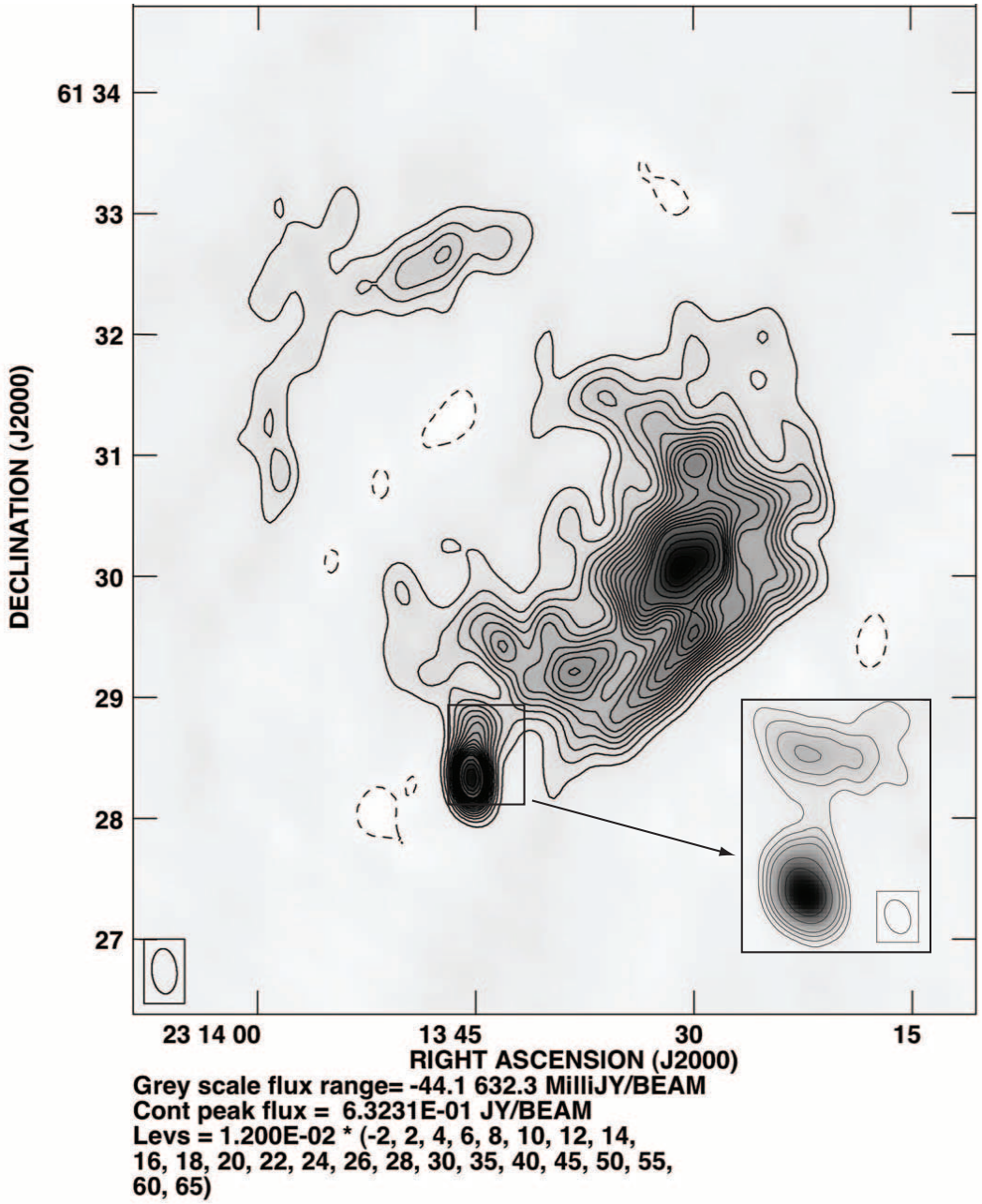

FIG. 2.—GMRT low-resolution map of the whole NGC 7538 region at 1280 MHz. The resolution is $22\farcs5 \times 12\farcs4$ along P.A. $= 4\fdg6$, and the rms noise in the map is $\sim$4 mJy beam^{-1}. The abscissa and the ordinate are in the J2000.0 epoch. The inset is a GMRT high-resolution map of the central radio peak. The image has a high resolution of $6\farcs6 \times 4\farcs7$ along P.A. $= 21\fdg4$, an rms of $\sim$1.3 mJy beam^{-1}, and a total flux density of 978.7 mJy. The lower part of the map is the same area as the JHK_s image (see Fig. 4).

ionization-bounded, while it is density-bounded toward the northeast.

3.3. *Photometric Analysis of Pointlike Sources*

3.3.1. *Color-Color Diagram*

We obtained photometric data of 1364 sources in J, 1679 in H, and 1682 in the K_s band. Figures 6*a* and 6*b* show the $J - H/H - K$ CC diagrams of the NGC 7538 star-forming region and the reference field, respectively, for the sources detected in the JHK_s bands with a positional agreement of less than $2''$ and with photometric errors in each color of less than 0.1 mag. The reference field is also used for the correction of field star contamination in the raw KLF of NGC 7538 (see § 3.5). In Figure 6, the solid and thick dashed curves represent the unreddened main-sequence and giant branches (Bessell & Brett 1988), and the parallel dashed lines are the reddening vectors for early- and late-type stars (drawn from the base and tip of the two branches). The dotted lines indicate the locus of T Tauri stars (Meyer et al. 1997). We have assumed that $A_J/A_V = 0.282$, $A_H/A_V = 0.175$, and $A_K/A_V = 0.112$ (Rieke & Lebofsky 1985). As can be seen in Figure 6*a*, the stars in NGC 7538 are distributed in a much wider range than those in the reference field (Fig. 6*b*), which indicates that a large fraction of the observed sources in NGC 7538 exhibit NIR excess emission characteristics of young stars with circumstellar material, as well as a wide range of reddening.

We classified the sources into three regions in the CC diagram (see, e.g., Tamura et al. 1998; Sugitani et al. 2002; Ojha

FIG. 3.—JHK_s composite image of the NGC 7538 star-forming region (J: *blue*; H: *green*; K_s: *red*) obtained with the three-color SIRIUS infrared array mounted on the University of Hawaii 2.2 m telescope. The FOV is $\sim 4'.9 \times 4'.9$. North is up, and east is to the left.

et al. 2004). "F" sources are located between the reddening vectors projected from the intrinsic color of main-sequence stars and giants and are considered to be field stars (main-sequence stars, giants) or Class III/Class II sources with small NIR excesses. "T" sources are located redward of region "F" but blueward of the reddening line projected from the red end of the T Tauri locus of Meyer et al. (1997). These sources are considered to be mostly classical T Tauri stars (Class II objects) with large NIR excesses. There may be an overlap in NIR colors of Herbig Ae/Be stars and T Tauri stars in the "T" region (Hillenbrand et al. 1992). "P" sources are those located in the region redward of region "T" and are most likely Class I objects (protostar-like objects). The total number of "T" (Class II) and "P" (Class I) sources are 268 and 18, respectively. By dereddening the stars on the CC diagram that fell within the reddening vectors encompassing the main-sequence and giant stars, we found the amount of visual extinction (A_V) for each star. The individual extinction values range from 0 to 40 mag with an average extinction of $A_V \sim 7$ mag.

3.3.2. *Color-Magnitude Diagram*

The CM diagram is a useful tool for studying the nature of the stellar population within star-forming regions and also for estimating its spectral types. Figure 7 is the $H - K$ versus K CM diagram, where all the sources detected in the JHK_s bands plus some 180 stars fainter than our limit at the J band but still above the detection threshold in the H and K_s bands are plotted. An apparent main-sequence track is noticeable with $A_V \sim 4$ mag in this diagram, but a comparison of it with a similar diagram for the stars in the reference field shows that it is a false sequence caused by field stars in the foreground of the NGC 7538 region. The vertical solid lines (from left to right in Fig. 7) represent the main-sequence curve reddened by $A_V = 0$, 20, 40, and 60 mag, respectively. We have assumed a distance of 2.8 kpc to the sources to reproduce the main-sequence data on this plot. The parallel slanting lines in Figure 7 trace the reddening zones for each spectral type. YSOs (Class II and I) found from the CC diagram (Fig. 6*a*) are shown as stars and triangles, respectively. However, it is important to note that even those sources not shown with stars or triangles may also be YSOs with an intrinsic color excess, since some of them are detected in the H and K_s bands only and are not in the J band because of their very red colors. The three bright and very red objects ($K < 12.0$, $H - K > 4.0$) located in the top right corner of the figure are the very young stars IRS 1, IRS 9, and IRS 9N1, in their earliest evolutionary phases (see § 3.8, Figs. 12*a* and

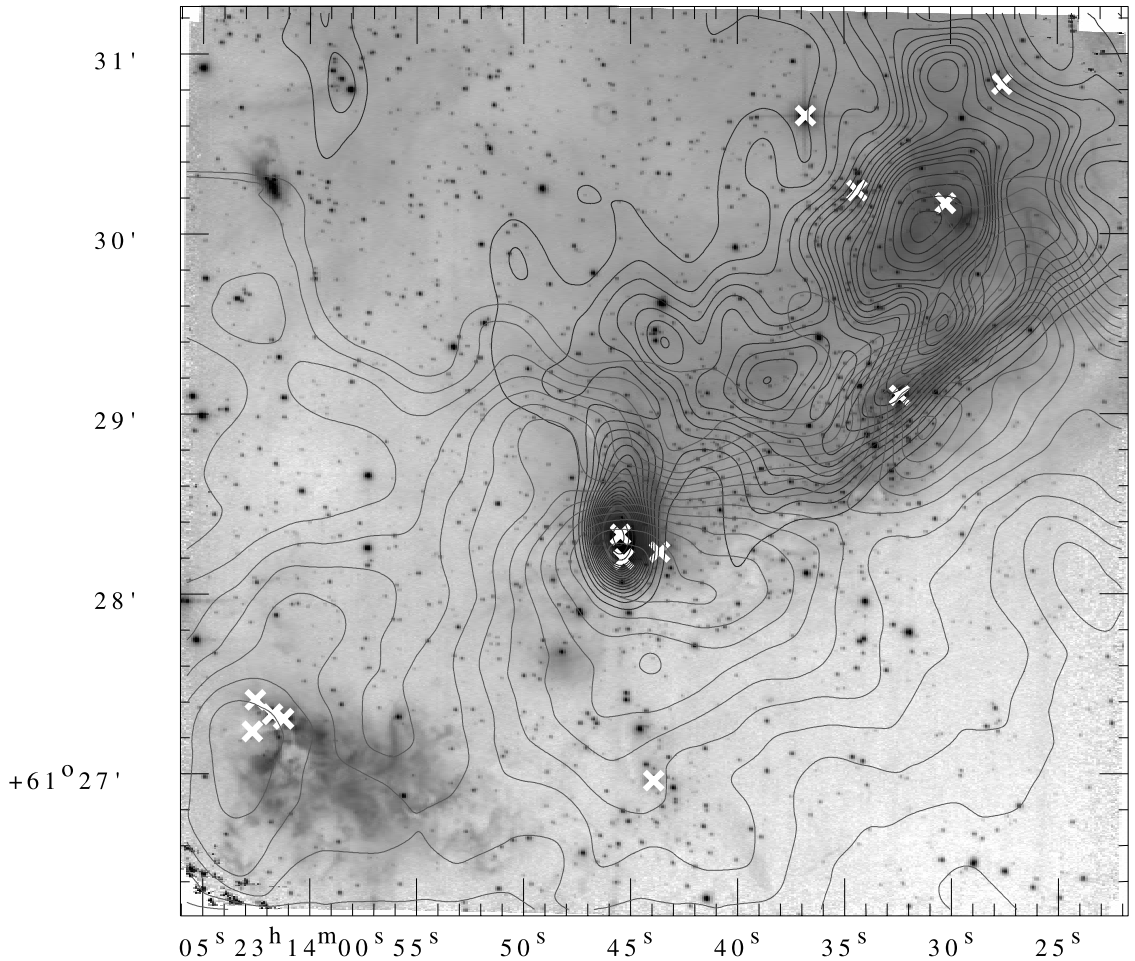

FIG. 4.—SIRIUS K_s-band image overlain by the GMRT radio continuum contours (*darker contours*). The lighter contours show the integrated emission of the CO ($J = 2-1$) line (from Davis et al. 1998). The CO contours start at 50 K km s^{-1} and increase in steps of 15 K km s^{-1}. The CO data were taken with the JCMT at $\sim 20''$ resolution. The positions of the IRS sources (see Table 1) are marked by crosses. The abscissa and the ordinate are in the J2000.0 epoch. [*See the electronic edition of the Journal for a color version of this figure.*]

12*b*). The bright infrared sources labeled as IRS numbers in Figure 7 are associated with the H II region and the molecular cloud (see Figs. 1, 4, and 5). These sources are shown in Table 1.

3.4. *Spatial Distribution of YSOs and Cool Red Sources*

In our deep NIR observations, 46 very red sources are detected only in the H and K_s bands. These sources have colors redder than $H - K > 2$ in Figure 7. In Figure 8, the spatial distribution of the YSO candidate sources identified in Figures 6*a* and 7 are shown. Blue stars represent sources of T Tauri type (Class II), filled green triangles indicate protostar-like objects (Class I), and filled red circles denote the very red sources ($H - K > 2$).

Most of the YSOs in NGC 7538 are arranged from the northwest to the southeast regions. Class II or T Tauri type objects and Class I or protostar-like objects (located in "T" and "P" regions in Fig. 6*a*, respectively) are distributed in the northwest and southeast regions over the field, but there is an apparent concentration of these sources mainly toward the northwest (the optically visible H II region). Class I sources are distributed along the interface between the optical H II region and the molecular cloud region to the west. Stars with large color indices ($H - K > 2$) are seen near the dense parts of the molecular cloud toward the south and southeast (Fig. 4; K. Sunada et al. 2004, in preparation). Most of them are clustered near the massive molecular clumps surrounding the luminous infrared sources IRS 1–3. Some of them are expected to be members of the embedded stellar clusters around IRS 1–3 and to the south of IRS 1–3 (i.e., around IRS 11). Therefore, these sources associated with the molecular clumps around IRS 9, IRS 11, and IRS 1–3 (K. Sunada et al. 2004, in preparation) are embedded pre–main-sequence (PMS) stars, presumably. A few red sources are also seen around the ionization front at the interface between the H II region and the molecular cloud, which might have formed because of the triggered star formation.

The average extinction through the molecular cloud in NGC 7538 that hosts the very red sources is $A_V \sim 15$ mag ($H - K \sim 1$). If we assume that the large $H - K$ (>2) color results merely from the interstellar reddening affecting normal stars, then the extinction value might even exceed 40 mag in the molecular cloud in which most of the red stars are found. However, with such a large amount of absorption, diffuse emissions are unlikely to be detected in the NIR. Since most of the red sources are associated with faint diffuse emission around IRS 1–3, IRS 9, and IRS 11, this provides evidence that these sources are YSOs with intrinsic NIR excesses and possibly local extinction as well. In Figure 7, a large fraction (~96%) of these sources are located above the straight line drawn from an A0 star parallel to the extinction vector. This suggests that they are intermediate-mass stars with circumstellar material.

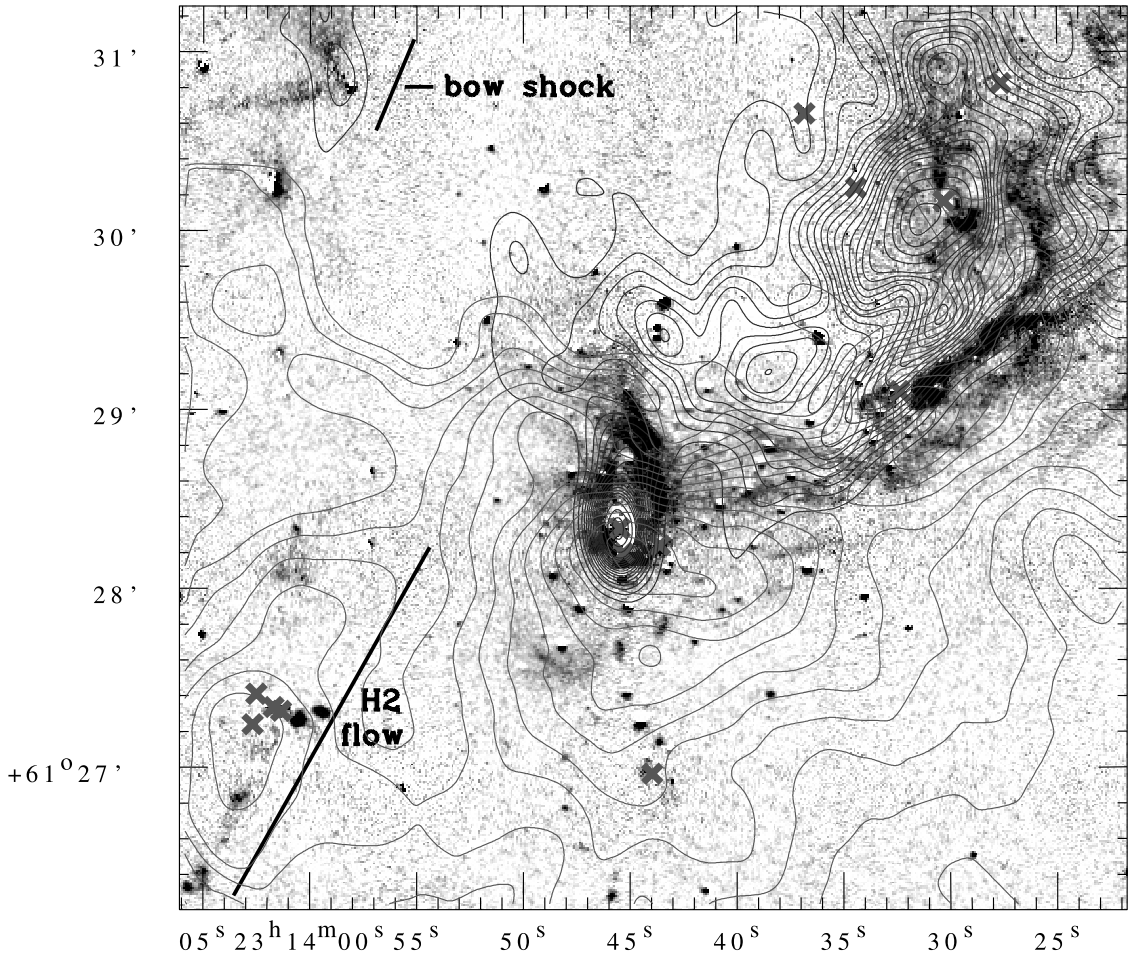

FIG. 5.—Continuum-subtracted molecular hydrogen emission at 2.122 μm of the NGC 7538 region (Davis et al. 1998). Residual artifacts left over by the subtraction of the 2.140 μm image from the 2.122 μm image are seen around the positions of some bright stars. The overlying contours and symbols are the same as those shown in Fig. 4. The direction of the IRS 9 "H_2 jet" in the southeastern corner and the bow shock region in the northeastern corner of the image are indicated. The abscissa and the ordinate are in the J2000.0 epoch. [*See the electronic edition of the Journal for a color version of this figure.*]

Based on the clustering of different YSO candidates in NGC 7538, the overall morphology is of three major condensations, which may form a sequence in age: the diffuse H II region (northwest, oldest), the compact IR core (center), and the regions with the extensive IR reflection nebula and a cluster of red young stars (southeast and south, youngest). This subject is further discussed in § 3.7.

3.5. *The K_s-Band Luminosity Function*

We use the KLF to constrain the initial mass function (IMF) and age of the embedded stellar population in NGC 7538. To derive the KLF, we have determined the completeness of the data through artificial star experiments using ADDSTAR in IRAF. This was performed by adding fake stars in random positions into the images at 0.5 mag intervals and then checking how many of the added stars could be recovered at various magnitude intervals. We repeated this procedure at least eight times. We thus obtained the detection rate as a function of magnitude, which is defined as the ratio of the number of recovered artificial stars to the number of added stars.

In order to estimate the foreground and background contaminations, we made use of both the Galactic model by Robin et al. (2003) and the reference field star counts. The star counts were predicted using the Besançon model of stellar population synthesis (Robin et al. 2003) in the direction of the reference field close to NGC 7538 (see § 2), which is also corrected for photometric completeness. By comparing the resulting model KLF with that of the reference field (see Fig. 9), we found that the simulation fits fairly well with the data. An advantage of using the model is that we can separate the contamination from the foreground ($d < 2.8$ kpc) and the background ($d > 2.8$ kpc) field stars. As we saw in § 3.4, the average extinction toward the NGC 7538 region is $A_V \sim 15$ mag ($H - K \sim 1$). Assuming spherical geometry, background stars are seen through $A_V \sim 30$ mag (2×15 mag). Therefore, we applied an extinction value of $A_V = 30$ mag (or $A_K = 3.36$ mag) in simulating the background stars. We combined the foreground and background stars to make a whole set of the contamination field and obtained the fraction of the contaminating stars over the total model counts. Then we scaled the model prediction to the star counts in the reference field, and subtracted the combined foreground ($d < 2.8$ kpc) and background ($d > 2.8$ kpc with $A_K = 3.36$ mag) data from the KLF of the NGC 7538 region.

After correcting for the foreground and background star contamination and photometric completeness, the resulting KLFs are presented in Figure 10 for the whole NGC 7538 region. They follow power laws in shape. In Figure 10, a power law with a slope α [$dN(m_K)/dm_K \propto 10^{\alpha m_K}$, where $N(m_K)$ is the number of stars brighter than m_K] has been fitted to each KLF (Figs. 10*a* and 10*b*) using a linear least-squares fitting routine.

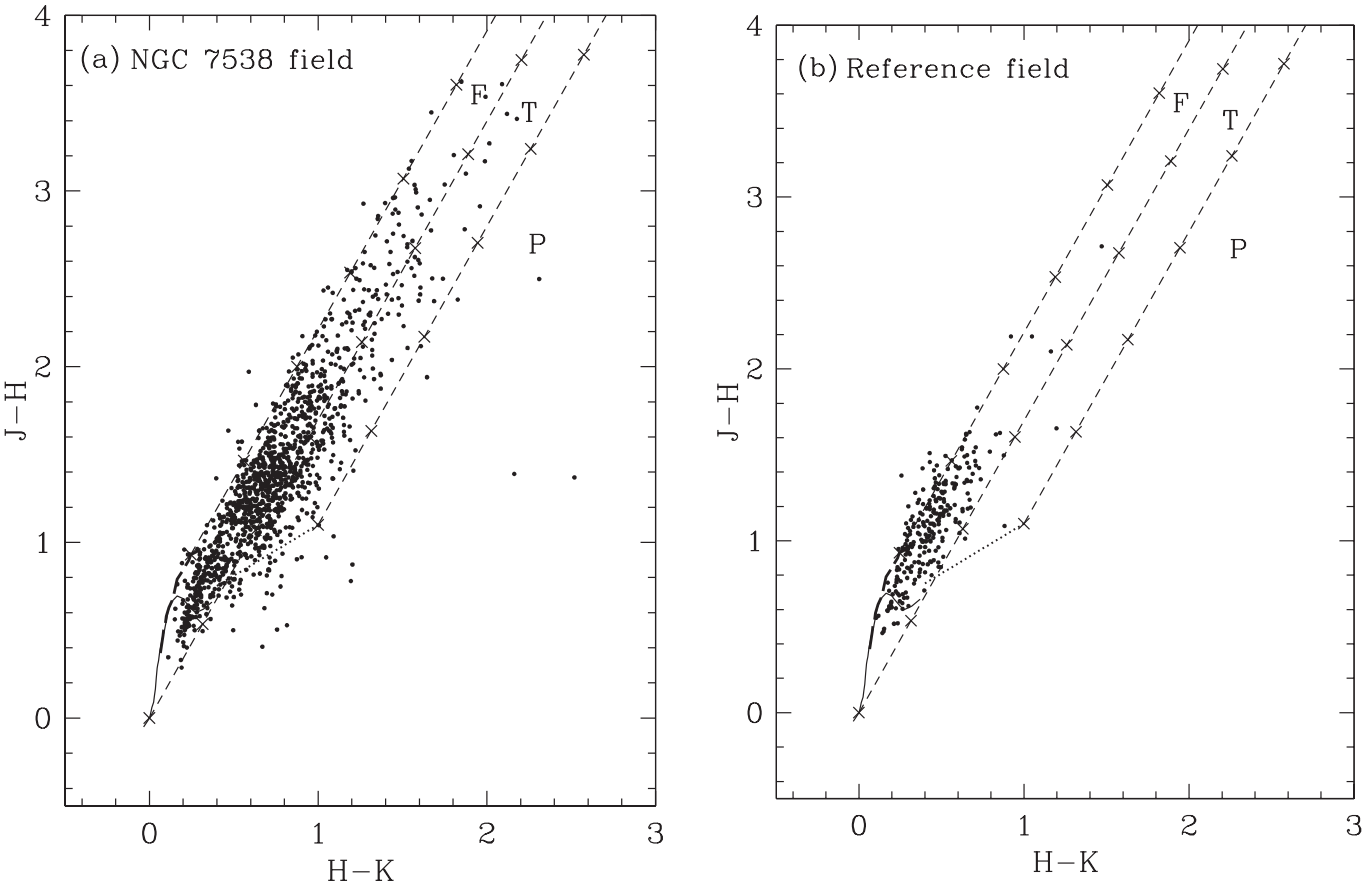

FIG. 6.—CC diagrams of (*a*) the NGC 7538 star-forming region and (*b*) the reference field for the sources detected in the JHK_s bands with photometric errors less than 0.1 mag. The sequences for field dwarfs (*solid curve*) and giants (*thick dashed curve*) are from Bessell & Brett (1988). The dotted line represents the locus of T Tauri stars (Meyer et al. 1997). Dashed straight lines represent the reddening vectors (Rieke & Lebofsky 1985). The crosses on the dashed lines are separated by $A_V = 5$ mag.

To discuss the relationship between the KLF slopes and the star-forming environment of each region, we divided the NGC 7538 region into two rectangular areas: the "younger" region (IRS 1–3, IRS 9, and IRS 11 regions) and the "older" region above IRS 1–3 (see Figs. 1 and 8, § 3.4). The derived power-law slopes for the younger, older, and whole NGC 7538 regions are shown in Table 2. We also note that the background subtraction does not significantly change the power-law slope (Fig. 10, Table 2).

We find a small increase (1 σ result; see Table 2) in the KLF slope from the younger region ($\alpha \sim 0.27$) to the most evolved older region ($\alpha \sim 0.33$) in NGC 7538 (see § 3.4). This is consistent with the expected change in the KLF slope with age if the IMF is identical in the whole NGC 7538 region (Megeath et al. 1996). However, such a small effect is not significant in view of the reddening and excess due to circumstellar material. Therefore, we assume a coeval population of stars and derive the KLF of the whole NGC 7538 star-forming region for comparison with other regions, as well as a rough estimate of stellar masses in the § 3.6.

The KLF of the whole NGC 7538 region shows a power-law slope that is lower than those generally reported for the young embedded clusters ($\alpha \sim 0.4$, e.g., Lada et al. 1991, 1993; Lada & Lada 2003), although equally low values have also been reported in the W3 Main star-forming region (Megeath et al. 1996; Ojha et al. 2004). Thus, this low value of the slope is indeed an intrinsic property of the stellar population in this region. Using the analysis given in detail by Megeath et al. (1996), the estimated KLF slope of the whole NGC 7538 region is roughly consistent with the Miller-Scalo IMF if the age of the NGC 7538 population is ~1 Myr.

3.6. *Stellar Mass Estimates*

Figure 11 shows the CM diagram ($J - H$ vs. J) for 286 YSO candidate sources identified in Figures 6*a* and 7. We estimate the mass of the stellar sources by comparing them with the evolutionary models of PMS stars (Palla & Stahler 1999). The solid curve in Figure 11 denotes the loci of 10^6 yr old PMS stars, and the dotted curve shows those of 0.3×10^6 yr old PMS stars. Masses range from 0.1 to 4 $M_\odot$ from bottom to top, for both curves. To estimate the stellar masses, we use the J luminosity rather than that of H or K_s, as the J band is less affected by the emission from circumstellar material (Bertout et al. 1988).

If the age of the NGC 7538 population is ~1 Myr, as estimated from the KLF slope (see § 3.5), ~88% of the YSO candidates detected in the J, H, and K_s bands have masses less than 3 $M_\odot$, and at least ~80% of the stars have masses less than 2 $M_\odot$ (Fig. 11). Even if the age of the stars is 0.3 Myr, ~92% of the stars have masses below 3 $M_\odot$. At the distance of 2.8 kpc, assuming an age of ~1 Myr and an extinction at the J band of up to ~2 mag ($A_V \sim 7$), the J-magnitude limit (corresponding to a 10 σ magnitude detection limit) corresponds to $M \sim 0.1\ M_\odot$, according to the PMS evolutionary tracks from Palla & Stahler (1999). This gives an estimate of the lowest mass limits of the

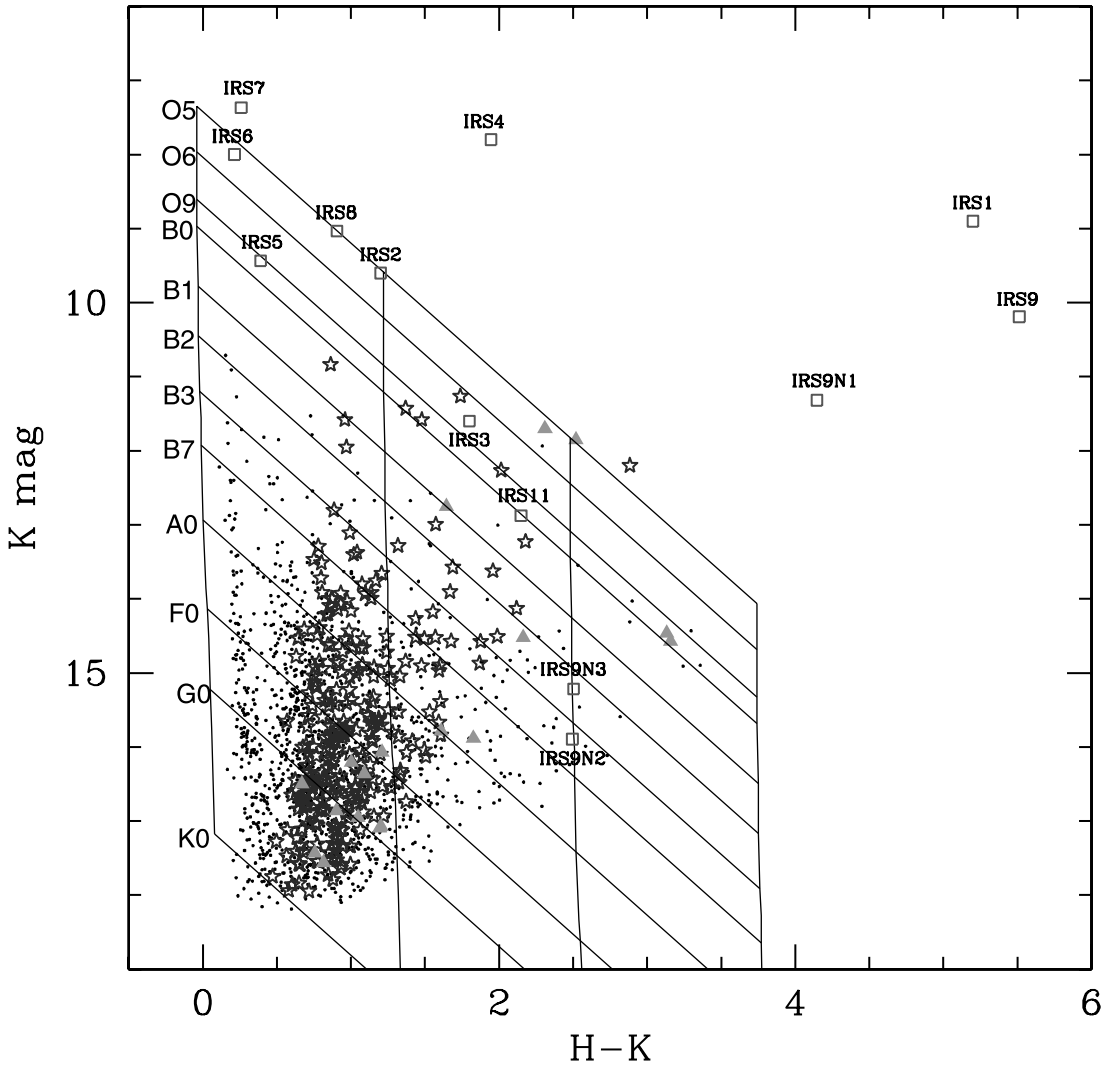

FIG. 7.—$H - K/K$ CM diagram for the sources detected in the H and K_s bands with photometric errors less than 0.1 mag. Stars and triangles represent the YSOs identified from the regions "T" and "P" in Fig. 6*a*, respectively. The vertical solid lines from left to right indicate the main-sequence track at 2.8 kpc reddened by $A_V = 0$, 20, 40, and 60 mag, respectively. The intrinsic colors are taken from Koornneef (1983). Slanting horizontal lines identify the reddening vectors (Rieke & Lebofsky 1985). Also shown are the positions of known IRS sources as open squares. [*See the electronic edition of the Journal for a color version of this figure*.]

TABLE 1

BRIGHT INFRARED SOURCES ASSOCIATED WITH THE H II REGION AND MOLECULAR CLUMP

Source	R.A. (J2000.0)	Decl. (J2000.0)	J (mag)	H (mag)	K (mag)	Spectral Type (From CM Diagram)
IRS 1	23 13 45.32	+61 28 11.7	...	14.10 ± 0.10[a]	8.90 ± 0.10[a]	...
IRS 2	23 13 45.47	+61 28 19.9	11.83 ± 0.06[b]	10.33 ± 0.08[b]	9.18 ± 0.10[b]	O5
IRS 3	23 13 43.65	+61 28 14.0	16.56 ± 0.04	13.63 ± 0.03	11.60 ± 0.10[a]	O6–O9
IRS 4	23 13 32.39	+61 29 06.2	...	9.74 ± 0.05[b]	7.80 ± 0.01[b]	...
IRS 5	23 13 30.24	+61 30 10.3	10.38 ± 0.03[b]	9.82 ± 0.04[b]	9.43 ± 0.04[b]	O9
IRS 6	23 13 34.38	+61 30 14.6	8.71 ± 0.02[b]	8.21 ± 0.04[b]	8.00 ± 0.01[b]	O5–O6
IRS 7	23 13 36.80	+61 30 39.6	8.44 ± 0.04[b]	7.63 ± 0.04[b]	7.37 ± 0.01[b]	...
IRS 8	23 13 27.58	+61 30 50.1	12.09 ± 0.02	9.94 ± 0.03[b]	9.03 ± 0.02[b]	O5
IRS 9	23 14 01.76	+61 27 19.9	...	15.70 ± 0.04	10.19 ± 0.05[b]	...
IRS 9N1	23 14 01.36	+61 27 18.4	19.79 ± 0.11	15.46 ± 0.08	11.32 ± 0.08[b]	...
IRS 9N2	23 14 02.70	+61 27 14.1	...	18.39 ± 0.08	15.89 ± 0.03	...
IRS 9N3	23 14 02.56	+61 27 24.6	...	17.72 ± 0.05	15.22 ± 0.07	...
IRS 9N4	23 14 02.40	+61 27 20.4	...	17.84 ± 0.11	15.39 ± 0.10	...
IRS 11	23 13 43.92	+61 26 57.8	18.50 ± 0.03	15.02 ± 0.03	12.88 ± 0.04	B0

NOTES.—Units of right ascension are hours, minutes, and seconds, and units of declination are degrees, arcminutes, and arcseconds. Sources are labeled as IRS numbers in Fig. 7.

[a] Magnitudes are from Bloomer et al. (1998).

[b] 2MASS magnitudes.

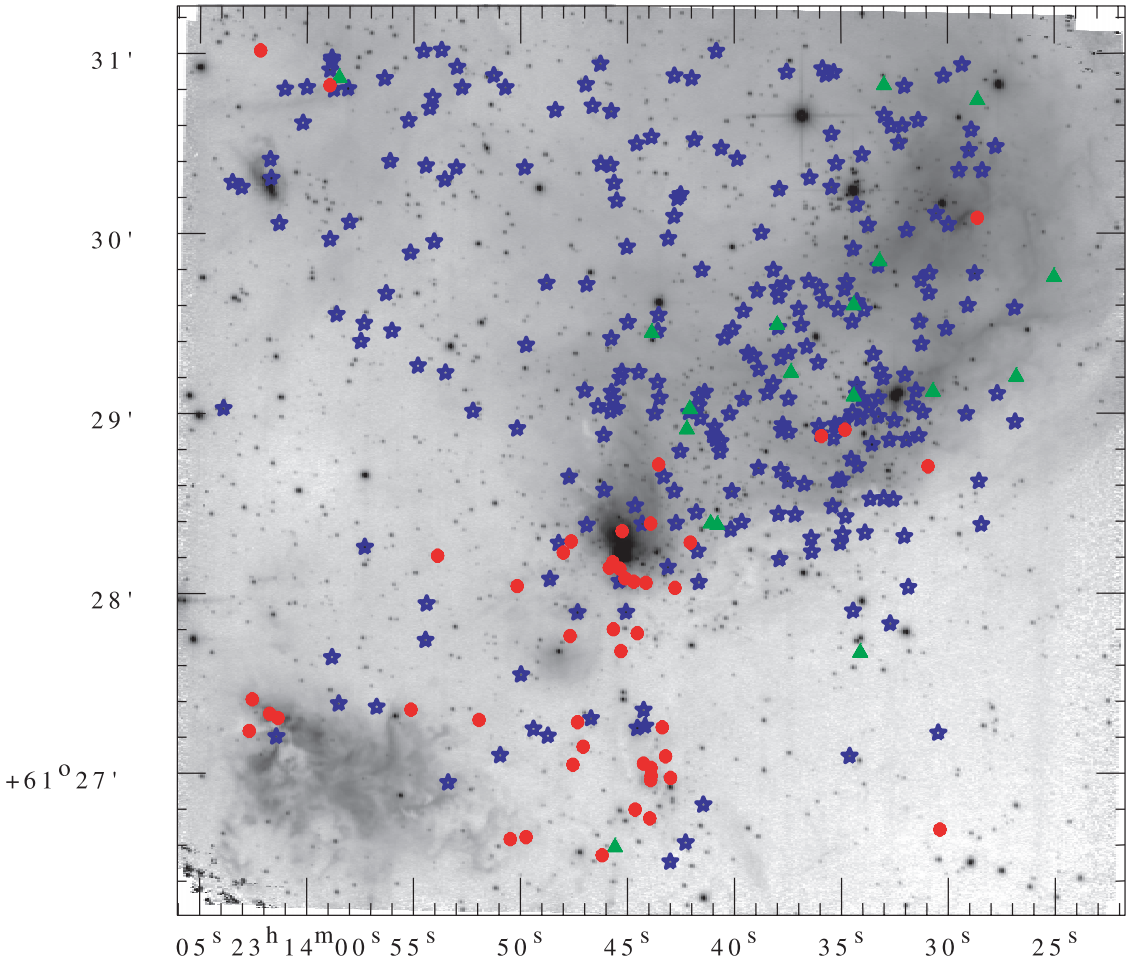

FIG. 8.—Spatial distribution of the YSO color-excess candidates superposed on the K_s-band image with a logarithmic intensity scale. Blue stars represent T Tauri and related sources (Class II), green triangles indicate Class I sources, and red circles denote the red sources ($H - K > 2$). The abscissa and the ordinate are in the J2000.0 epoch.

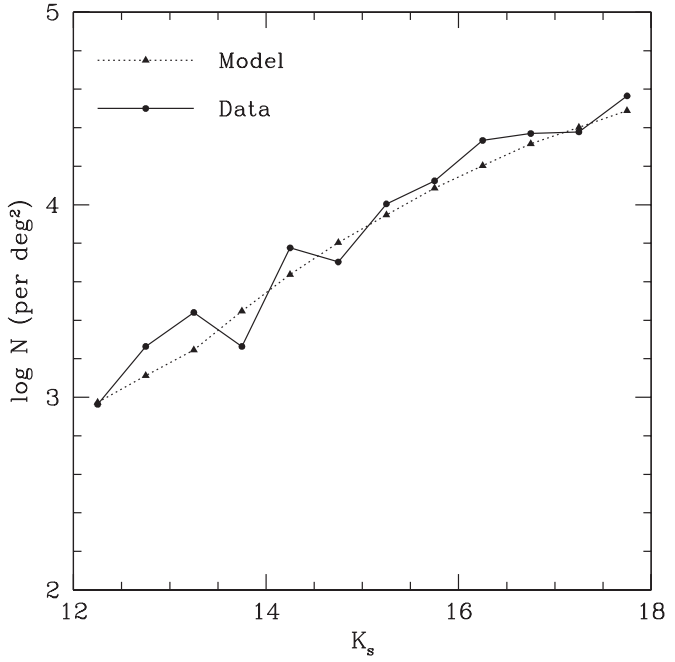

FIG. 9.—Comparison of the observed KLF in the reference field and the simulated KLF from star count modeling. The circles and solid line denote the K-band star counts in the reference field, and the triangles and dotted line represent the simulation from the Galactic model (see the text). The KLF slope (α, see § 3.5) of the dotted line (model simulation) is 0.29 ± 0.01.

detected stars in the NGC 7538 star-forming region in our sample.

Therefore, the stellar population in NGC 7538 may be primarily composed of low-mass PMS stars similar to those observed in the W3 Main star-forming region (Ojha et al. 2004). We also see the presence of lower mass stars forming the clusters (e.g., near the IRS 1–3 and IRS 4–8 regions) together with the newly formed O–B type stars. These results further support the hypothesis that the formation of high-mass stars is associated with the formation of clusters of low-mass stars (e.g., Lada & Lada 1991; Zinnecker et al. 1993; Persi et al. 1994; Tapia et al. 1997; Ojha et al. 2004).

3.7. *Star Formation Activity in NGC 7538*

The NGC 7538 star-forming complex seems to be composed of several structures of different evolutionary stages aligned from northwest to southeast. The first is the northwestern region, which corresponds to the visible H II region. Here, in addition to the optically visible O-type stars (e.g., IRS 5 and 6) we detect a large number of Class II and Class I sources (see Fig. 8). This northwestern region is undoubtedly more evolved than other regions of the NGC 7538 complex, which contain the majority of red sources but, in contrast, a far smaller number of Class II and Class I sources. Presumably the star-forming activity has already ended in this region except for the interface with the molecular cloud to the southwest, where we notice a few red sources.

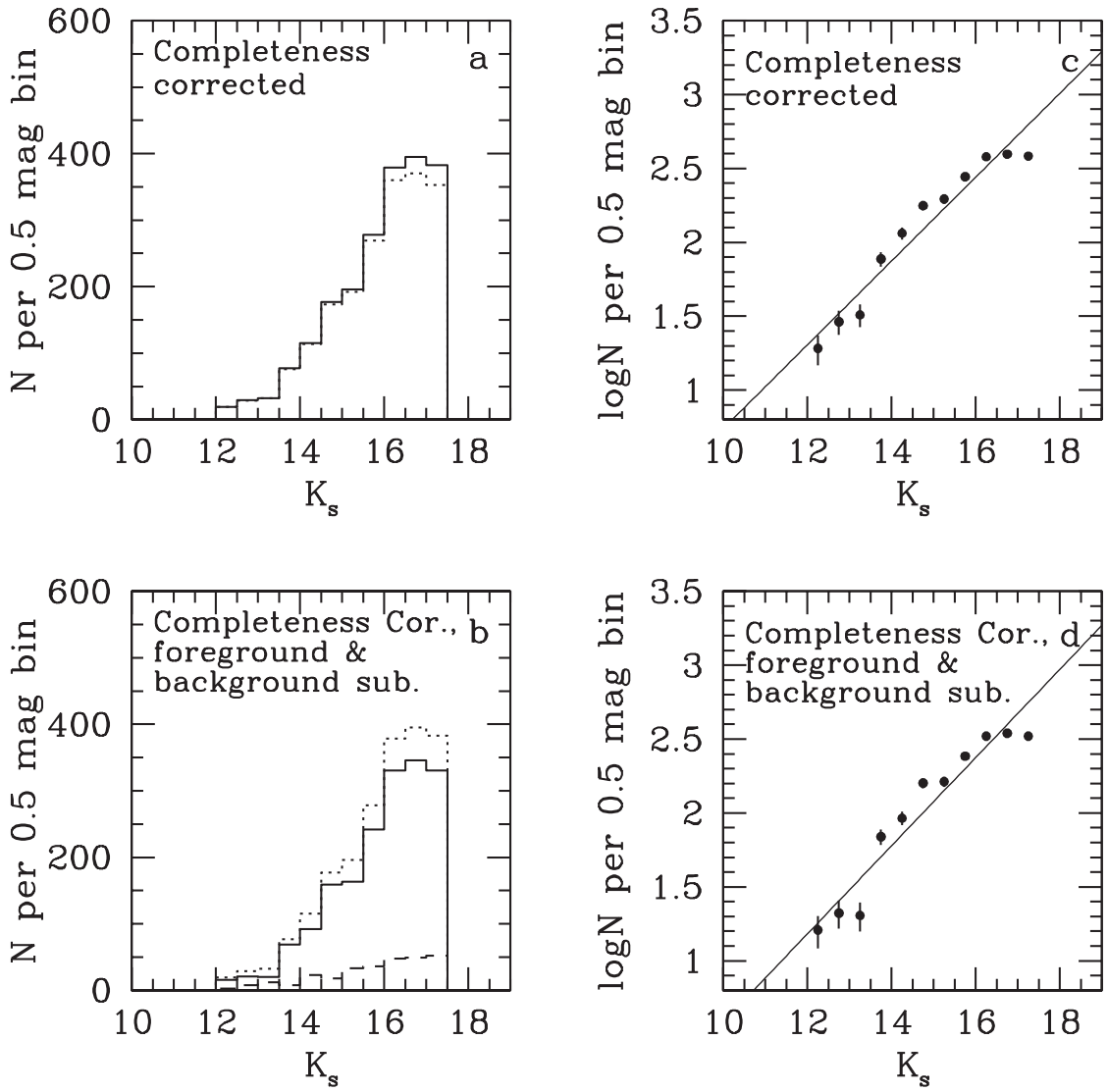

FIG. 10.—(*a*, *b*) Corrected KLF for the whole NGC 7538 region. In (*a*), the dotted line denotes the raw KLF, and the solid line shows the KLF corrected only for completeness. In (*b*), the dotted line shows the KLF corrected only for completeness. The dashed line denotes the field star counts from the reference field corrected for completeness and modified to reflect the unextincted foreground and background stars reddened by $A_V = 30$ mag ($A_K = 3.36$ mag), with the help of the Galactic model (Robin et al. 2003). The solid line corresponds to the field star–subtracted KLF. (*c*, *d*) Logarithm of the completeness-corrected and field star–subtracted KLF of the NGC 7538 region, respectively. The solid lines are the best linear fit to the data points.

Second, a distinct core of star-forming activity is found near the center of our survey area. This is a compact region around IRS 1–3 surrounded by the bright IR nebula. These IR sources are all newly formed OB star candidates. Together with the (ultra-) compact H II regions that they have started to develop, they are deeply embedded in the dense molecular core. Here we also notice a concentration of red sources. Most probably extensive star-forming activity is currently taking place in this region.

Turning our eyes farther to the southeast, we find a rather scattered distribution of red sources and Class II candidates. We propose that they compose the third region of star-forming activity in the NGC 7538 complex. It seems to be composed of two substructures; one corresponds to the fluffy reflection nebula associated with IRS 9, 9N1, 9N2, and 9N3 (the southeastern region), and the other is the region surrounding IRS 11 and an elongated grouping of red stars (the southern region). The extensive reflection nebula is a manifestation of massive

TABLE 2
POWER-LAW FITS TO KLFS IN NGC 7538

Region	α	Correction
Whole NGC 7538	0.28 ± 0.02	Completeness corrected
	0.30 ± 0.03	Completeness corrected, foreground and background subtracted
Younger (IRS 1–3, 9, and 11)	0.27 ± 0.03	
Older (optical H II)	0.33 ± 0.04	

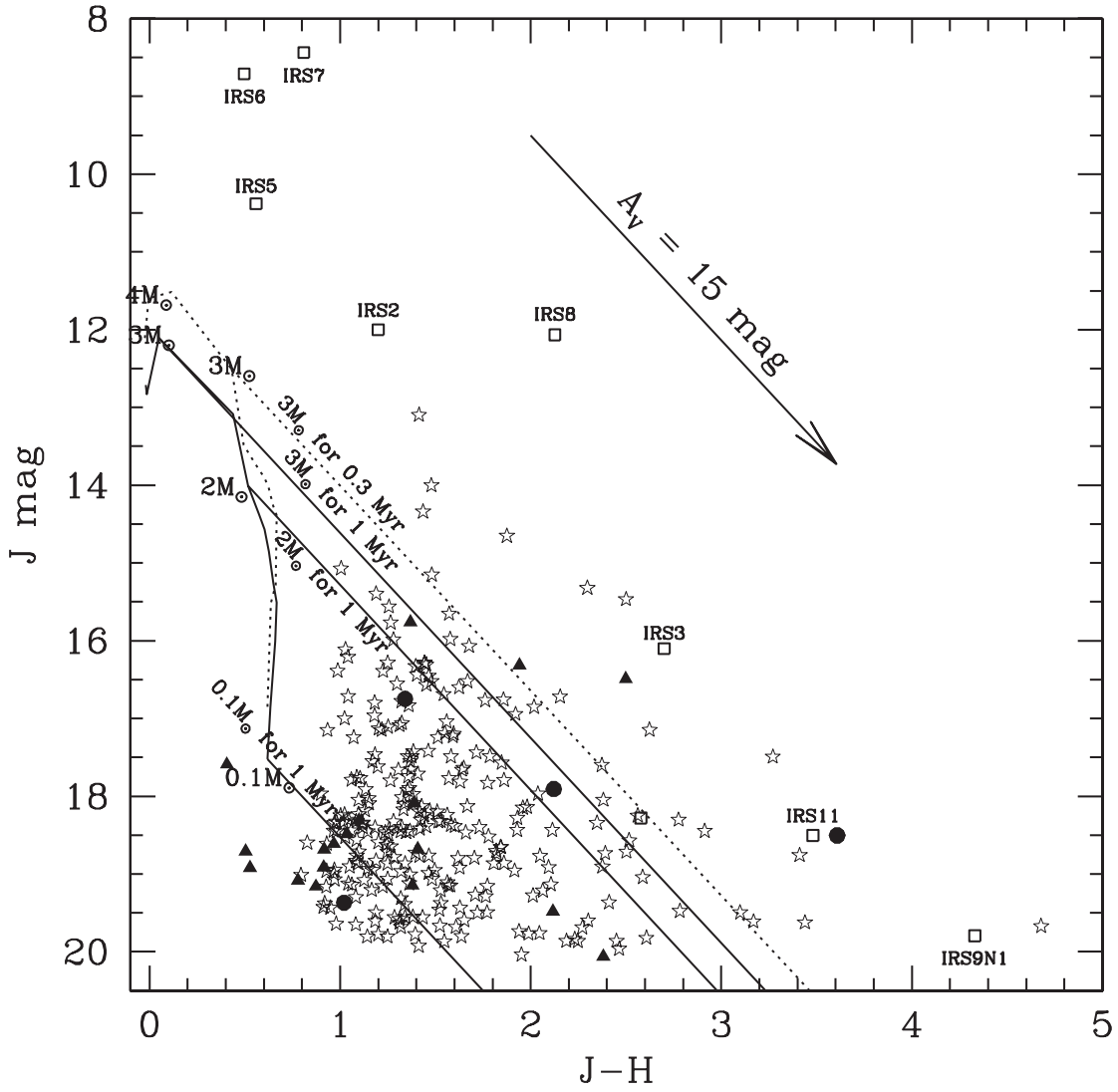

FIG. 11.—CM diagram for the YSO candidates in NGC 7538. Class II candidates are indicated by stars, triangles represent Class I candidates, and circles show red sources with $H - K > 2$ with J-band counterparts. The solid curve denotes the loci of 10^6 yr old PMS stars, and the dotted curve is for those that are 0.3×10^6 yr old; both were derived from the model of Palla & Stahler (1999). Masses range from 0.1 to 4 $M_\odot$ from bottom to top, for both curves. The dotted oblique reddening line denotes the position of a PMS star of 3 $M_\odot$ for 0.3 Myr, and the solid oblique lines denote the positions of PMS stars of 0.1, 2, and 3 $M_\odot$ for 1 Myr. Most of the objects well above the PMS tracks are luminous and massive ZAMS stars (see Table 1, Fig. 7).

outflows associated with IRS 9 (Tamura et al. 1991). The presence of massive outflows associated with IRS 9 and the existence of masers and NGC 7538S (Class 0 candidate, § 3.8.3) around IRS 11 are clear signs of an early phase of star formation in these regions. Therefore, this third region, both southeastern and southern, is located in the molecular cloud and must be very young in terms of star formation.

The question can then be raised: What is the time sequence of the star formation history in NGC 7538? The central region appears to be the result of the propagation of star formation activity from the northwest region due to the expansion of the H II region and the compression of the molecular cloud in the northwestern interface. Its location adjacent to the NGC 7538 H II region and the dense concentration of YSOs between the H II region and the IRS 1–3 core match quite well the characteristics of sequential star formation (Elmegreen & Lada 1977). The complex to the south and southeast might have evolved independently from the same molecular cloud. Since this region is separated from the optical H II region of NGC 7538, the star formation here is independent of the action of its expansion and appears to have been taking place spontaneously, as suggested by McCaughrean et al. (1991). Alternatively, it could be possible that some larger scale trigger might have played a role, resulting in the entire sequence of these three stages of star formation activity. In order to answer this question, however, it might be crucial to reveal the YSO population on a much larger scale.

3.8. *Individual Sources and Regions*

In Figure 12 we present some selected areas of the NGC 7538 star-forming region in our high-resolution (0.″7) NIR images that are of particular interest.

3.8.1. *IRS 1, 2, and 3*

NGC 7538 IRS 1–3 is a group of three infrared sources in the very bright red core in the center of the image (Fig. 12*a*). These three high-luminosity infrared sources are located at the boundary of the H II region (see Fig. 1). They were found in a

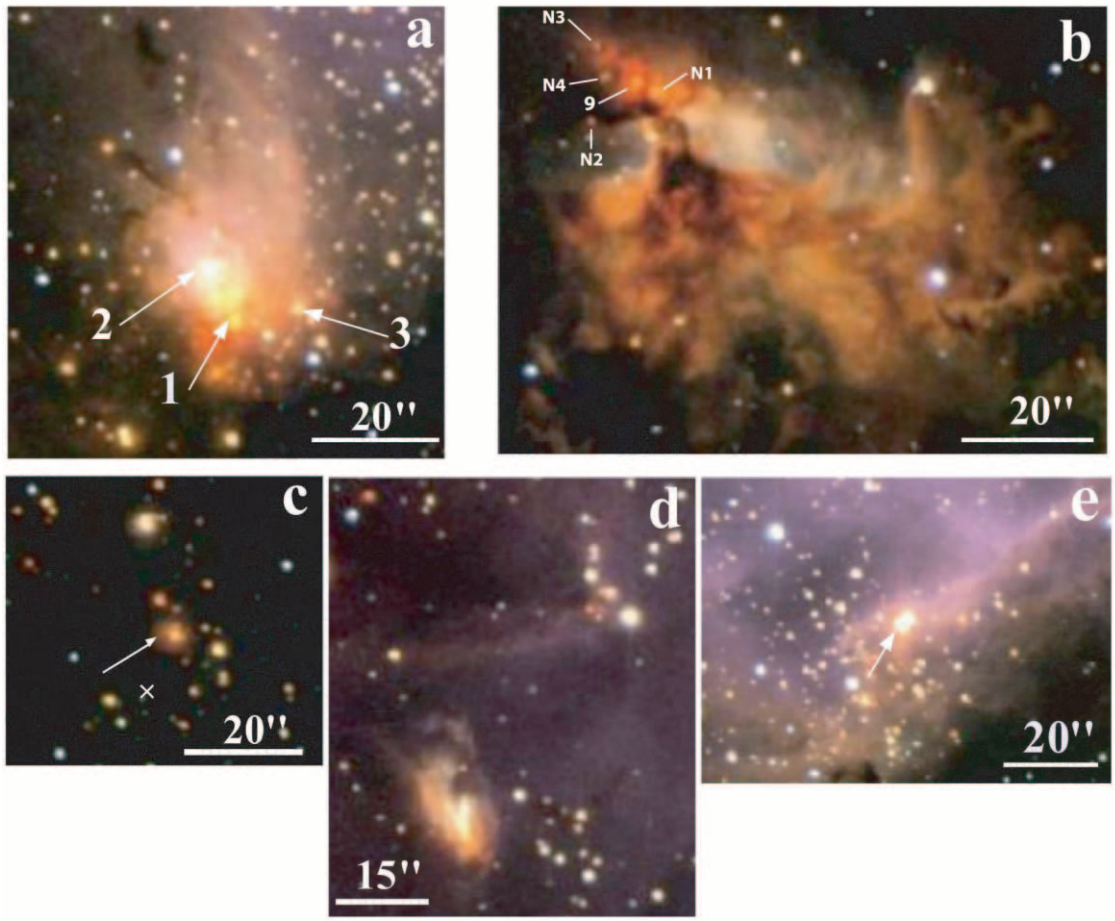

FIG. 12.—Enlarged view of the color image of selected areas (see Fig. 3, § 3.8). (*a*) NGC 7538 IRS 1–3 region. The three high-luminosity infrared sources IRS 1–3 are located at the boundary of the H II region. (*b*) Striking reflection nebula in the southeastern corner of our JHK_s image in Fig. 3. NGC 7538 IRS 9 is a bright and pointlike infrared source at the apex of the complex reflection nebula (marked by "9"). In its immediate vicinity three more extremely red infrared sources, IRS 9N1, IRS 9N2, and IRS 9N3, are located (marked by "N1," "N2," and "N3"; see § 3.8.2). (*c*) NGC 7538 IRS 11 (marked by an arrow), most likely a young star associated with a nebulosity. The cross shows the 850 μm position of NGC 7538S (a high-mass Class 0 candidate). (*d*) Small peculiar nebulosities seen in the northeast corner of our JHK_s image in Fig. 3. The northern one shows a cone-shaped silhouette enveloped by a faint nebulosity, probably due to bow-shaped H_2 emission (see Fig. 5; Davis et al. 1998). The southern one shows an oval shape overlain by dark patches. (*e*) Barely resolved double source NGC 7538 IRS 4 (*arrowed*) associated with the local nebulosity, which is located toward the northwest of IRS 2 at the boundary of the optical H II region.

2.2 and 20 μm survey of NGC 7538 (Wynn-Williams et al. 1974), southeast of the optical H II region. IRS 1 is identified as a UC H II region, while IRS 2 and 3 are compact and optically thin compact H II regions, respectively (Campbell 1984; Campbell & Persson 1988). IRS 2 is embedded in the center of the compact IR nebula, whereas IRS 1 and IRS 3 are located near the south and southwestern borders of the nebula, respectively (Fig. 12*a*).

IRS 1 is the most luminous ($L_{\rm NIR} = 1.5 \times 10^5\ L_\odot$; Willner 1976; Hackwell et al. 1982) of the three infrared sources. This source is detected only in the H and K_s bands among our images (Table 1). The high spatial resolution submillimeter data resolved the young UC H II region around IRS 1, and it was shown that the UC H II region is surrounded by a cluster of submillimeter sources, none of which have near- or mid-infrared counterparts (Sandell & Sievers 2004). We see an elongated group of red stars in a filamentary structure around IRS 1 in our NIR image (see Fig. 8). IRS 2, inferred to be an O9.5 zero-age main-sequence (ZAMS) star with a luminosity of $\sim 3.8 \times 10^4\ L_\odot$ (Campbell & Persson 1988; Campbell & Thompson 1984) based on its ionizing flux, is situated $\sim 10''$ north of IRS 1 and possesses the most extended H II region of the cluster sources. A red star is located about $2''$ northwest of IRS 2 (Fig. 8). IRS 3, the least luminous of the cluster sources, is situated about $15''$ west of IRS 1. No red stars are seen close to IRS 3 (Fig. 8).

3.8.2. *IRS 9 Reflection Nebula*

Located about $2'$ southeast of IRS 1, IRS 9 is a bright, pointlike IR source at the apex of a complex reflection nebula (marked by "9" in Fig. 12*b*). IRS 9 is detected only in our H- and K_s-band images (Table 1). The CO outflow driven by IRS 9 (Kameya et al. 1989) is associated with extensive H_2 emission (Fig. 5; Davis et al. 1998). Sandell & Sievers (2004) found IRS 9 to be extended and disklike in their high spatial resolution submillimeter maps. The total mass of the IRS 9 submillimeter source is $\sim 150\ M_\odot$. The bolometric luminosity of IRS 9 is $\sim 2 \times 10^4\ L_\odot$ (Werner et al. 1979; Thronson & Harper 1979).

The striking reflection nebula in Figure 12*b* is associated with IRS 9 (Werner et al. 1979; Tamura et al. 1991), which shows very delicate and complex features of structure and color. This suggests a complex structure of circumstellar material and its massive YSOs.

At the easternmost tip of the nebula, four extremely red infrared sources including IRS 9 are located (Fig. 12*b*; see also Fig. 8). We designate these sources as IRS 9N1, IRS 9N2, and

IRS 9N3 (see Figs. 1 and 7, Table 1). Two of them near the tip are associated with a "silhouette shell." While comparing with the polarization map (Tamura et al. 1991), we find that IRS 9N1 is probably not an independent source but is most likely an unresolved gaseous knot in the nebula, because the degree of polarization is very high at the position of IRS 9N1, and the polarization pattern is not disturbed. For other sources (IRS 9N2 and 9N3) the polarization is locally small, or the pattern is disturbed. These red sources, as well as a nearby bluer source IRS N4 (marked by "N4" in Fig. 12*b*; see Table 1), are most probably very young stars in their earliest evolutionary phases and appear to be associated with small-scale circumstellar matter that obscures the background nebula (we call this matter silhouette shells). It is possible that the kinematics of the IRS 9 region is influenced by these YSOs (Sandell & Sievers 2004).

3.8.3. *IRS 11 and NGC 7538 S*

IRS 11 is situated $\sim 1'$ south of IRS 1 (marked by an arrow in Fig. 12*c*). This IRS source is associated with a tiny nebulosity (Fig. 12*c*) and a knot of vibrationally excited H_2 emission (Davis et al. 1998), suggesting that it is most likely a young star with an outflow. Kameya et al. (1989) also reported a CO outflow in this region. The CO outflow associated with IRS 11 appears poorly collimated, however, roughly aligned with that associated with IRS 1. A large number of red young stars are also seen around the IRS 11 region (Fig. 8). This fact, together with the results of the submillimeter polarimetry by Momose et al. (2001), indicates that the IRS 11 region is younger than the IRS 1 region.

NGC 7538S [$(\alpha, \delta) = (23^{\rm h}13^{\rm m}44^{\rm s}.51, +61^\circ 26' 48''.7)$ (J2000.0) at 850 μm], a high-mass Class 0 candidate, is about 80″ to the south of IRS 1 (the 850 μm position is shown by a cross in Fig. 12*c*; Sandell & Sievers 2004). These authors resolved the submillimeter emission into an elliptical source (NGC 7538 S) of $14'' \times 7''$, P.A. $= 58^\circ \pm 3^\circ$. We find two very red sources associated with this elliptical source [$(\alpha, \delta) = (23^{\rm h}13^{\rm m}44^{\rm s}.65, +61^\circ 26' 47''.9)$ and $(23^{\rm h}13^{\rm m}43^{\rm s}.96, +61^\circ 26' 44''.9)$ (J2000.0); see Figs. 8 and 12*c*]. However, they are unlikely to be the counterparts to the submillimeter source, considering the Class 0 nature of NGC 7538 S. The existence of NGC 7538S and a concentration of red sources further support the conclusion that the southern region is younger than other regions in NGC 7538.

3.8.4. *Bow Shock Region?*

Figure 12*d* is a section in the northeast corner of our JHK_s image in Figure 3, where we detect peculiar nebulosities. The northern one shows a cone-shaped silhouette enveloped by a faint nebulosity, probably due to bow-shaped H_2 emission (Fig. 5; Davis et al. 1998). The southern one shows an oval shape overlain by dark patches and is associated with at least two YSOs (see Fig. 8). This nebula is within a local deep obscuration in an optical image. About 40″ north of this object a bow-shaped structure of H_2 emission, which is made of two elongations, one in the east-west direction and the other in the north-south direction, is found (Fig. 5; see also Fig. 7 of Davis et al. 1998). This structure is presumably caused by an outflow from the northeast of this region.

3.8.5. *NGC 7538 IRS 4*

Figure 12*e* shows the barely resolved double source IRS 4 (separation $\sim 1''.4$) in our NIR images (marked by an arrow in the center of the image). It is an isolated red source ($H - K = 1.94$) associated with local nebulosity, which is located toward the northwest of IRS 2 at the boundary of the optical H II region.

A faint, extended dust condensation was seen about 15″ to the southwest of IRS 4 in an 850 μm map (Sandell & Sievers 2004). These authors also found a fainter extended submillimeter source near the 20 μm source IRS 4. IRS 4, in view of its significant 20 μm flux, is most probably a compact H II region. It is also situated close to a knot in the ammonia emission and appears to be close to the interface between the H II region and the molecular cloud (Zheng et al. 2001).

4. CONCLUSIONS

A subarcsecond JHK_s-band NIR imaging survey of YSOs associated with the NGC 7538 star-forming region is presented. The survey covers a $4'.9 \times 4'.9$ area down to a limiting magnitude (10 σ) of $J = 19.5$, $H = 18.4$, and $K_s = 17.3$. The NIR images presented in this work are deeper than any *JHK* surveys to date for the larger area of the NGC 7538 star-forming region. From the analysis of these images we derive the following conclusions.

1. We see several different evolutionary stages in the NGC 7538 star-forming complex with considerable substructure, as also suggested by McCaughrean et al. (1991). There are lines of evidence for sequential star formation in NGC 7538.
2. Most of the YSOs in NGC 7538 are arranged from the northwest to the southeast regions, which form a sequence in age: the diffuse H II region (northwest and oldest, where most of the Class II and Class I sources are detected), the compact IR core (center), and the regions with the extensive IR reflection nebula and a cluster of red young stars (southeast and south).
3. A large number of red stars ($H - K > 2$) are detected in the NGC 7538 molecular cloud region, most of which are clustered around the molecular clumps associated with IRS 1–3 and toward the south and southeast of IRS 1–3.
4. The YSOs in the central region are probably the results of the propagation of star-forming activity from the northwestern region due to the expansion of the H II region and the compression of the molecular cloud (sequential star formation; Elmegreen & Lada 1977). The southeastern/southern region is independent of the above action, and presumably the star formation there is taking place in a spontaneous and gradual process.
5. The KLF of the whole NGC 7538 region shows a power-law slope of $\alpha = 0.30 \pm 0.03$, which is lower than the typical values reported for embedded young clusters, although equally low values have also been reported in the W3 Main star-forming region. We also find a small increase in the KLF slope from the younger region ($\alpha \sim 0.27$) to the most evolved older region ($\alpha \sim 0.33$) in NGC 7538. The resulting KLF slopes may therefore indicate the age sequence of various regions in NGC 7538.
6. Using the age of $\sim$1 Myr, we find that about 88% of the YSO candidates have an upper mass limit of 3 $M_\odot$. We estimate that the lowest mass limit of Class II and Class I candidates in our observations is 0.1 $M_\odot$. Therefore, the stellar population in NGC 7538 is primarily composed of low-mass PMS stars.
7. The radio continuum image based on the GMRT observations at 1280 MHz shows interesting morphological details, including an arc-shaped structure highlighting the interaction between the H II region and the adjacent molecular cloud. The ionization front at the interface between the H II region and the molecular cloud is clearly seen by comparing the radio continuum, molecular line, and molecular hydrogen images. It is most plausible that NGC 7538 IRS 6 is the main exciting source responsible for the H II region.

It is a pleasure to thank the anonymous referee for a most thorough reading of this paper and several useful comments and suggestions, which greatly improved the scientific content of the paper. We thank the staff of the University of Hawaii 2.2 m telescope for supporting the first run of SIRIUS. D. K. O. was supported by the Japan Society for the Promotion of Science through a fellowship, during which most of this work was done. We acknowledge support by Grants-in-Aid (10147207, 12309010, and 13573001) from the Ministry of Education, Culture, Sports, Science, and Technology. We thank the staff of the GMRT who made the radio observations possible. The GMRT is run by the National Centre for Radio Astrophysics of the Tata Institute of Fundamental Research (India). We thank Francesco Palla for providing us with the PMS grids. We thank Annie Robin for letting us use her model of stellar population synthesis. We thank Chris Davis for providing us with the FITS images of his H_2, narrowband K continuum, and CO molecular line observations of NGC 7538. This publication makes use of data products from the Two Micron All Sky Survey, which is a joint project of the University of Massachusetts and the Infrared Processing and Analysis Center, California Institute of Technology, funded by the National Aeronautics and Space Administration and the National Science Foundation.

REFERENCES

Akabane, K., Matsuo, H., Kuno, N., & Sugitani, K. 2001, PASJ, 53, 821
Bertout, C., Basri, G., & Bouvier, J. 1988, ApJ, 330, 350
Bessell, M. S., & Brett, J. M. 1988, PASP, 100, 1134
Blitz, L., Fich, M., & Stark, A. A. 1982, ApJS, 49, 183
Bloomer, J. D., et al. 1998, ApJ, 506, 727
Campbell, B. 1984, ApJ, 282, L27
Campbell, B., & Persson, S. E. 1988, AJ, 95, 1185
Campbell, B., & Thompson, R. I. 1984, ApJ, 279, 650
Davis, C. J., Moriarty-Schieven, G., Eislöffel, J., Hoare, M. G., & Ray, T. P. 1998, AJ, 115, 1118
Dickel, H. R., Rots, A. H., Goss, W. M., & Forster, J. R. 1982, MNRAS, 198, 265
Elmegreen, B. G., & Lada, C. J. 1977, ApJ, 214, 725
Gaume, R. A., Johnston, K. J., Nguyen, H. A., Wilson, T. L., Dickel, H. R., Goss, W. M., & Wright, M. C. H. 1991, ApJ, 376, 608
Hackwell, J. A., Grasdalen, G. L., & Gehrz, R. D. 1982, ApJ, 252, 250
Hillenbrand, L. A., Strom, S. E., Vrba, F. J., & Keene, J. 1992, ApJ, 397, 613
Kameya, O., Hasegawa, T. I., Hirano, N., Takakubo, K., & Seki, M. 1989, ApJ, 339, 222
Kameya, O., Morita, K.-I., Kawabe, R., & Ishiguro, M. 1990, ApJ, 355, 562
Koornneef, J. 1983, A&A, 128, 84
Lada, C. J., & Lada, E. A. 1991, in ASP Conf. Ser. 13, The Formation and Evolution of Star Clusters, ed. K. Janes (San Francisco: ASP), 3
———. 2003, ARA&A, 41, 57
Lada, C. J., Young, E. T., & Greene, T. P. 1993, ApJ, 408, 471
Lada, E. A., Evans, N. J., Depoy, D. L., & Gatley, I. 1991, ApJ, 371, 171
Madden, S. C., Irvine, W. M., Matthews, H. E., Brown, R. D., & Godfrey, P. D. 1986, ApJ, 300, L79
McCaughrean, M., Rayner, J., & Zinnecker, H. 1991, Mem. Soc. Astron. Italiana, 62, 715
Megeath, S. T., Herter, T., Beichman, C., Gautier, N., Hester, J. J., Rayner, J., & Shupe, D. 1996, A&A, 307, 775
Menten, K. M., Walmsley, C. M., Henkel, C., & Wilson, T. L. 1986, A&A, 157, 318
Meyer, M., Calvet, N., & Hillenbrand, L. A. 1997, AJ, 114, 288
Momose, M., Tamura, M., Kameya, O., Greaves, J. S., Chrysostomou, A., Hough, J. H., & Morino, J.-I. 2001, ApJ, 555, 855
Moreno, M. A., & Chavarria, K. C. 1986, A&A, 161, 130
Nagashima, C., et al. 1999, in Proc. Star Formation 1999, ed. T. Nakamoto (Nagano: Nobeyama Radio Obs.), 397
———. 2003, MNRAS, 343, 1263
Nagayama, T., et al. 2003, Proc. SPIE, 4841, 459
Ojha, D. K., et al. 2004, ApJ, 608, 797
Palla, F., & Stahler, S. 1999, ApJ, 525, 772
Persi, P., Roth, M., Tapia, M., Ferrari-Toniolo, M., & Marenzi, A. R. 1994, A&A, 282, 474
Persson, S. E., Murphy, D. C., Krzeminski, W., Roth, M., & Rieke, M. J. 1998, AJ, 116, 2475
Rieke, G. H., & Lebofsky, M. J. 1985, ApJ, 288, 618
Robin, A. C., Reylé, C., Derrière, S., & Picaud, S. 2003, A&A, 409, 523
Rots, A. H., Dickel, H. R., Forster, J. R., & Goss, W. M. 1981, ApJ, 245, L15
Sandell, G., & Sievers, A. 2004, ApJ, 600, 269
Sandell, G., Wright, M., & Forster, J. R. 2003, ApJ, 590, L45
Stetson, P. B. 1987, PASP, 99, 191
Sugitani, K., et al. 2002, ApJ, 565, L25
Swarup, G., Ananthakrishnan, S., Kapahi, V. K., Rao, A. P., Subrahmanya, C. R., & Kulkarni, V. K. 1991, Curr. Sci., 60, 95
Tamura, M., Gatley, I., Joyce, R. R., Ueno, M., Suto, H., & Sekiguchi, M. 1991, ApJ, 378, 611
Tamura, M., Itoh, Y., Oasa, Y., & Nakajima, T. 1998, Science, 282, 1095
Tapia, M., Persi, P., Bohigas, J., & Ferrari-Toniolo, M. 1997, AJ, 113, 1769
Thronson, H. A., Jr., & Harper, D. A. 1979, ApJ, 230, 133
Werner, M. W., Becklin, E. E., Gatley, I., Matthews, K., Neugebauer, G., & Wynn-Williams, C. G. 1979, MNRAS, 188, 463
Willner, S. P. 1976, ApJ, 206, 728
Wood, D. O. S., & Churchwell, E. 1989, ApJS, 69, 831
Wynn-Williams, C. G., Becklin, E. E., & Neugebauer, G. 1974, ApJ, 187, 473
Zheng, X. W., Zhang, Q., Ho, P. T. P., & Pratap, P. 2001, ApJ, 550, 301
Zinnecker, H., McCaughrean, M. J., & Wilking, B. A. 1993, in Protostars and Planets III, ed. E. Levy & J. Lunine (Tucson: Univ. Arizona Press), 429